

A Comparative Study of Three Different Bounce-Back Scheme Based Methods for a Moving Curved Solid Boundary Implementation in the Lattice Boltzmann Method

M. Beigzadeh-Abbassi¹, M. Taeibi-Rahni², M.R. Beigzadeh-Abbassi² and A.R. Beigzadeh-Abbassi³

¹Mechanical Engineering Department, Sirjan University of Technology, Sirjan, Iran

²Aerospace Engineering Department, Sharif University of Technology, Tehran, Iran

³Institut für Land- und Seeverkehr (ILS), Technische Universität Berlin, Berlin, Germany
m.r.beigzadeh@gmail.com

Abstract: Accurate simulation of curved solid boundaries is of great importance in lattice Boltzmann method, because solid curved boundaries are used in many applications, such as turbine blades, airfoils, curved body of flying objects, depositing solid particles, blood flow in vessels, flow round heat exchanger pipes, etc. In lattice Boltzmann method, curved boundary was first simulated by using standard bounce-back boundary condition. This boundary condition was not able to simulate curved boundary accurately. Lots of corrections have been made so far to improve the bounce-back boundary condition for curved solid boundary [1]. In this study three of these corrections are compared with each other in respect of accuracy and stability. These boundary conditions are: (1) FH boundary condition, (2) mass conserving FH boundary condition, and (3) OSIF boundary condition. Numerical results obtained from simulations a two-dimensional flow over a stationary and moving circular cylinder, also simulation a flow over a transitional oscillating circular cylinder show that FH boundary condition predicts more accurate and more acceptable results in comparison with the other two boundary conditions. Therefore to simulate moving curved solid boundary in applicational problems, FH boundary condition can be used with assurance.

[M. Beigzadeh-Abbassi, M. Taeibi-Rahni, M.R. Beigzadeh-Abbassi and A.R. Beigzadeh-Abbassi. A **Comparative Study of Three Different Bounce-Back Scheme Based Methods for a Moving Curved Solid Boundary Implementation in the Lattice Boltzmann Method**. Journal of American Science 2012;8(3):218-227]. (ISSN: 1545-1003). <http://www.americanscience.org>. 29

Keywords: Lattice Boltzmann method; Curved Boundary Condition; Bounce-back Boundary Condition; Unsteady Flow

1. Introduction

In the last decade, scientists proposed many algorithms for simulating curved solid boundary condition in lattice Boltzmann method. Most of these methods are basically different with each other but most of them are modified versions of previous methods. Curved solid boundary was first simulated using standard bounce-back boundary condition. Standard bounce-back boundary condition used to simulate curved solid boundary in a stair-shaped manner and was not able to simulate curved solid boundary condition accurately.

Some of the modifications, which were made to standard bounce-back boundary condition are:

(1) FH Boundary Condition: Filippova, O. and Hanel (1998) have offered a second-order accuracy model for simulating curved solid boundary in lattice Boltzmann method. They have used this boundary condition with locally fined lattices to simulate flow over a circular cylinder in two different cases, one a steady flow with Reynolds number 20 and the other an unsteady flow with Reynolds number 100 [2],

(2) Mass Conserving FH Boundary Condition: Bao, J., Yuan, P. and Schaefer, L. (2008) have presented a new boundary condition with

second-order accuracy which is a modified version of FH boundary condition. They claim that they have improved the mass conservation problem from which the FH boundary condition suffers [3], and

(3) OSIF Boundary Condition: This boundary condition was offered by Kao, P.H. and Yang, R. J. (2008) and it has a big difference with the other two boundary conditions because no interpolation is used in this boundary condition. Those boundary conditions in which interpolation is used suffer from mass-leakage. The authors claim that by using this boundary condition mass-leakage error has been reduced and the value of calculated transferred momentum has been modified [4].

As far as we know, a study in which bounce-back scheme based boundary conditions have been compared with each other has not been published, yet. This study will provide us with a powerful comparative tool according to which we can choose a suitable and accurate boundary condition for simulating applicational problems.

2. Lattice Boltzmann Method

Lattice Boltzmann method has been constructed according to dynamics of particles and uses Boltzmann equation which has a mesoscopic

concept (a concept between microscopic and macroscopic) instead of using Navier-stokes equations which has a macroscopic basis [5]. Spacial and temporal differencing of Boltzmann equation and resulting to lattice Boltzmann equation has been summarized in the following. Beginning from Boltzmann equation we have [6]:

$$\frac{Df_\alpha}{Dt} = \frac{\partial f_\alpha}{\partial t} + \mathbf{e}_\alpha \cdot \nabla f_\alpha = \Gamma^{(+)} - \Gamma^{(-)} \tag{1}$$

Using Bhatnagar-Gross-Krook (BGK) approximation, the collision operator has been linearized:

$$\frac{Df_\alpha}{Dt} = \frac{\partial f_\alpha}{\partial t} + \mathbf{e}_\alpha \cdot \nabla f_\alpha = -\frac{1}{\lambda} (f_\alpha - f_\alpha^{(eq)}), \tag{2}$$

where $f_\alpha^{(eq)}$ is Maxwell-boltzmann equilibrium function. Using finite difference, the material derivative in the left hand side of equation (2) is differenced as:

$$\frac{Df_\alpha}{Dt} = \frac{f_\alpha(\mathbf{x} + \mathbf{e}_\alpha \Delta t, t + \Delta t) - f_\alpha(\mathbf{x}, t)}{\Delta t} = -\frac{1}{\lambda} (f_\alpha - f_\alpha^{(eq)}). \tag{3}$$

By introducing non-dimensional relaxation time, lattice Boltzmann equation is derived [6]:

$$\tau = \Delta t / \lambda, \tag{4}$$

$$f_\alpha(\mathbf{x} + \mathbf{e}_\alpha \Delta t, t + \Delta t) - f_\alpha(\mathbf{x}, t) = -\frac{1}{\tau} (f_\alpha - f_\alpha^{(eq)}). \tag{5}$$

Equation (5) is known as lattice Boltzmann equation, which is separated into two steps to be solved numerically. One step is the collision step (right hand side of equation (5)) and the other is the streaming step (left hand side of equation (5)) of the distribution function (f). Density and velocity of the fluid can be obtained from distribution functions by these equations [7]:

$$\rho = \sum_{\alpha=0}^8 f_\alpha, \tag{6}$$

$$\mathbf{u} = \frac{1}{\rho} \sum_{\alpha=0}^8 f_\alpha \mathbf{e}_\alpha. \tag{7}$$

2.1. Two-Dimensional Model Using D2Q9 Lattice

D2Q9 lattice uses a two-dimensional nine-velocity lattice. This method has been introduced by Qian et al. (1992). In this model particles are allowed to reside only on lattice nodes. The velocities of particles are limited to three values and their directions are limited to eight values [8] (figure 1).

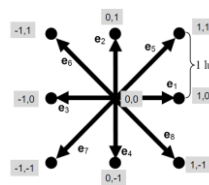


Figure 1. D2Q9 x, y velocity components [6]

2.2. FH Boundary Condition

The fraction of the intersected link in the fluid region is [2]:

$$\Delta = \frac{|\mathbf{x}_f - \mathbf{x}_w|}{|\mathbf{x}_f - \mathbf{x}_b|}, \tag{8}$$

which is illustrated in Figure 2.

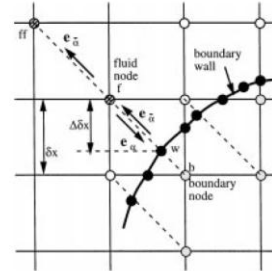


Figure 2. Cartesian two-dimensional lattices and solid curved boundary [2]

To finish the streaming step, it is clear that $f_\alpha^{\%}(\mathbf{x}_b, t)$ should be calculated and then substituted as:

$$f_\alpha(\mathbf{x}_f = \mathbf{x}_b + \mathbf{e}_\alpha \delta t, t + \delta t) = f_\alpha^{\%}(\mathbf{x}_b, t). \tag{9}$$

Filippova and Hanel have obtained the value of $f_\alpha^{\%}(\mathbf{x}_b, t)$ by using a linear interpolation of the information of neighboring nodes:

$$f_\alpha^{\%}(\mathbf{x}_b, t) = (1 - \chi) f_\alpha^{\%}(\mathbf{x}_f, t) + \chi f_\alpha^{(*)}(\mathbf{x}_b, t), \tag{10}$$

where $f_\alpha^{(*)}(\mathbf{x}_b, t)$ is known as fictitious equilibrium function and is defined by the following equation:

$$f_\alpha^{(*)}(\mathbf{x}_b, t) = \omega_\alpha \rho(\mathbf{x}_f, t) \left[1 + \frac{3}{c^2} \mathbf{e}_\alpha \cdot \mathbf{u}_{bf} + \frac{9}{2c^4} (\mathbf{e}_\alpha \cdot \mathbf{u}_f)^2 - \frac{3}{2c^2} \mathbf{u}_f \cdot \mathbf{u}_f \right], \tag{11}$$

where the parameter ω_i is a weighting factor specific for each velocity direction. In the case of the D2Q9, $\omega_0 = 4/9$, $\omega_1 = 1/9$, and $\omega_2 = 1/36$ where ω_0 is the coefficient for the rest velocity, ω_1 is the coefficient for velocity directions with a magnitude of one (1, 2, 3, and 4 in this case), and ω_2 is the coefficient for velocity directions with a magnitude of $\sqrt{2}$ (5, 6, 7, and 8 in this case). The value of c is defined as, $c = \Delta x / \Delta t$, which has a magnitude of one in this model.

Filippova and Hanel have introduced the values of χ and \mathbf{u}_{bf} for different values of Δ :

$$\mathbf{u}_{bf} = (\Delta - 1) \mathbf{u}_f / \Delta + \mathbf{u}_w / \Delta, \quad \chi = (2\Delta - 1) / \tau, \tag{12}$$

$$\text{for } \Delta \geq 1/2, \tag{13}$$

$$\text{and } \mathbf{u}_{bf} = \mathbf{u}_f, \quad \chi = (2\Delta - 1) / (\tau - 1), \tag{14}$$

$$\text{for } \Delta \leq 1/2. \tag{15}$$

2.3. Mass Conserving FH Boundary Condition

Mass conserving FH boundary condition is very similar to FH boundary condition just in term of fictitious distribution function. In this boundary condition fictitious distribution function is modified in order to guarantee the conservation of mass [3]:

$$f_{\alpha}^{(*)}(\mathbf{x}_b, t) = w_{\alpha} \rho(\mathbf{x}_w, t) \left[1 + \frac{3}{c^2} \mathbf{e}_{\alpha} \cdot \mathbf{u}_{bf} + \frac{9}{2c^4} (\mathbf{e}_{\alpha} \cdot \mathbf{u}_{bf})^2 - \frac{3}{2c^2} \mathbf{u}_f \cdot \mathbf{u}_f \right], \tag{16}$$

where $\rho(\mathbf{x}_w, t)$ is known as wall density. The value of $\rho(\mathbf{x}_w, t)$ depends on the geometry of wall and the geometry of lattice. As an example we think of a two-dimensional flat channel. As illustrated in figure 3, for a D2Q9 lattice and for the lower part of a two-dimensional flat channel after the streaming step the numerical values of f_4, f_7 and f_8 are known and the numerical values of f_2, f_3 and f_6 are unknown which must to be calculated.

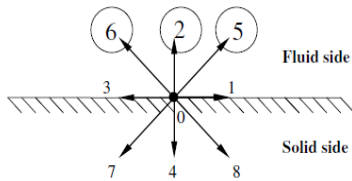


Figure 3. f_4, f_7, f_8 :Outgoing distribution functions, $f_2 = ? f_3 = ?, f_6 = ?$: Incoming distribution functions [3]

To satisfy conservation of mass the following equation must be satisfied:

$$\sum_{\text{outgoing}} f = \sum_{\text{incoming}} f. \tag{17}$$

In the above equivalence the unknown distribution functions are substituted by equation (16). After substitution and some calculations and simplifications the following equation is obtained:

$$f_4 + f_7 + f_8 = \frac{1}{6} \rho(\mathbf{x}_w, t) [1 - 3u_{bf}^y + 3(u_f^y)^2], \tag{18}$$

where, u_{bf}^y and u_f^y are y components of velocity vectors \mathbf{u}_{bf} and \mathbf{u}_f , respectively. So the value of $\rho(\mathbf{x}_w, t)$ can be obtained:

$$\rho(\mathbf{x}_w, t) = 6 \frac{f_4 + f_7 + f_8}{1 - 3u_{bf}^y + 3(u_f^y)^2}. \tag{19}$$

By satisfying the equation $\sum_{\text{outgoing}} f = \sum_{\text{incoming}} f$ in this boundary condition, total mass of the system during solution approach would be conserved.

2.4. OSIF Boundary Condition (a Non-interpolation Boundary Condition for Solid Curved Boundary)

As shown in Figure 4, for an instance of the proposed interpolation-free model, the distribution functions directed toward the curved boundary, i.e. f_3, f_4 , and f_7 , are treated as the values from “coarse” grid transferring into the “fine” grid:

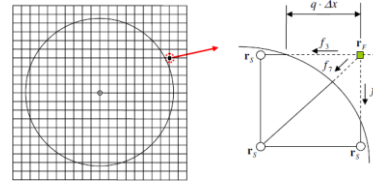


Figure 4. Illustration of interpolation-free treatment of curved boundary using local refinement concept [4]

When transferring information between nodes associated with different lattice sizes, it is essential to rescale the distribution functions at each link (f_i) in order to satisfy the principles of mass and momentum conservation, respectively, and to ensure a continuity of the deviatoric stresses across the interface between the two different grids. In rescaling the distribution functions, the following grid size ratio is defined:

$$Q' \equiv \frac{\Delta x^{(f)}}{\Delta x^{(c)}}. \tag{20}$$

where superscripts (c) and (f) denote the coarse grid and the fine grid quantities, respectively. To ensure a consistent viscosity and Reynolds number in the coarse lattice ($\Delta x^{(c)}$) and fine lattice ($\Delta x^{(f)}$), the relationship between the two relaxation factors of the two different lattices must conform to:

$$\begin{aligned} \nu_c = \nu_f &\Rightarrow \left(\frac{2}{\omega^{(c)}} - 1\right) \Delta x^{(c)} \frac{c}{6} = \left(\frac{2}{\omega^{(f)}} - 1\right) \Delta x^{(f)} \frac{c}{6} \\ &\Rightarrow \left(\frac{2}{\omega^{(c)}} - 1\right) \frac{1}{Q'} = \left(\frac{2}{\omega^{(f)}} - 1\right) \Rightarrow \omega^{(f)} = \frac{2Q'}{Q' + \left(\frac{2}{\omega^{(c)}} - 1\right)}, \end{aligned} \tag{21}$$

where $\omega^{(c)}$ and $\omega^{(f)}$ are the relaxation parameters of course and fine lattices, respectively. Furthermore, the derivatives of the distribution functions must be continuous across the interface between the two different grids. Consequently, the following relationship is applied between the post-collision distribution functions ($f_i^{\%}$) at adjacent nodes in the coarse and fine lattices [4]:

$$f_i^{\% (f)} = f_i^{(eq)} + (f_i^{\%} - f_i^{(eq)}) \cdot \frac{Q' \omega^{(c)} (1 - \omega^{(f)})}{\omega^{(f)} (1 - \omega^{(c)})}. \tag{22}$$

In the proposed model, the boundary fluid distribution function is rescaled according to equation (22) and is then streamed to the surface of the solid node \mathbf{r}_w in the propagation step, i.e. the $f(\mathbf{r}_w, t + \Delta t)$. The on-site BB scheme is then applied at the solid surface, i.e. by setting

$$f_{-i}^0(\mathbf{r}_w, t + \Delta t) = f_i(\mathbf{r}_w, t + \Delta t) \quad (23)$$

in the following collision step. Finally, the distribution function is streamed back to the fluid node in the subsequent propagation step to obtain $f_{-i}(\mathbf{r}_F, t + 2\Delta t)$ at time-level $(t + 2Dt)$.

2.5. Zou, Q and He, X. Boundary Condition on a Flow Boundary with Fixed Velocity

Suppose a flow boundary (take the inlet in Figure 1 as example) is along the y -direction, and the pressure (density) is to be specified on it. After streaming, f_2, f_3, f_4, f_6 and f_7 are known, u_x and u_y are specified at inlet. (the velocity profile is the velocity profile of a poisson flow).

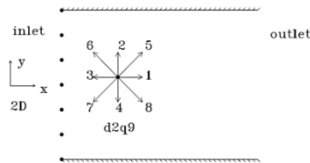


Figure 5. Boundary nodes in inlet boundary for a two-dimensional channel flow [10]

By solving the four equations obtained from equations of mass, momentum and the equation obtained from bounce-back rule for the non-equilibrium part of the particle distribution normal to the inlet, density and other unknown distribution functions are obtained:

$$\rho = \frac{1}{1-u_x} [f_0 + f_2 + f_4 + 2(f_3 + f_6 + f_7)], \quad (24)$$

$$f_1 = f_3 + \frac{2}{3}\rho u_x, \quad (25)$$

$$f_5 = f_7 - \frac{1}{2}(f_2 - f_4) + \frac{1}{2}\rho u_y + \frac{1}{6}\rho u_x, \quad (26)$$

$$f_8 = f_6 + \frac{1}{2}(f_2 - f_4) - \frac{1}{2}\rho u_y + \frac{1}{6}\rho u_x. \quad (27)$$

2.6. Calculating the Force on a Body

By using the momentum-exchange method presented by Ladd & Verberg the force exerted on a surface by fluid can be evaluated [11]. The force exerted on a boundary can be evaluated using the distribution function after the collision step and the

momentum exchange term which relates to the object velocity (figure 6).

$$\mathbf{F}(\mathbf{x}_w, t + \frac{1}{2}\Delta t) = \frac{\Delta x^3}{\Delta t} [2f_i^c(\mathbf{x}_A, t) - \frac{2w_i\rho(\mathbf{u}_w \cdot \mathbf{e}_i)}{c_s^2}] \mathbf{e}_i. \quad (28)$$

where the parameter w_i is a weighting factor.

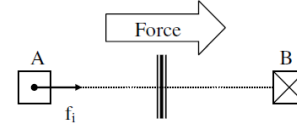


Figure 6. Illustration of the Momentum-Exchange Method for Force Evaluation (fluid exists only outside of wall) [11]

In order to get the total force and torque on a solid moving particle immersed in fluid, a summation of the forces is done around the boundary of a particle [11]:

$$\mathbf{F}_{total}(t + \frac{1}{2}\Delta t) = \sum \mathbf{F}(\mathbf{x}_w, t + \frac{1}{2}\Delta t), \quad (29)$$

$$\mathbf{T}_{total}(t + \frac{1}{2}\Delta t) = \sum (\mathbf{x}_w - \mathbf{x}_{CM}) \times \mathbf{F}(\mathbf{x}_w, t + \frac{1}{2}\Delta t). \quad (30)$$

In order to compare different boundary conditions with each other for a moving solid curved boundary at first we compare these boundary conditions for a stationary solid curved boundary.

3. Steady Two-dimensional Flow with Reynolds Number 20 over a Circular Cylinder in a Channel

In figure 7 the geometry of the flow domain and its boundary conditions are shown. The width of the channel is $H=0.41m$ and the diameter of the cylinder is $D=0.1m$ [13]. The Reynolds number in this problem is defined as:

$$Re = \bar{U}D/\nu, \quad (31)$$

where $\bar{U}(t) = 2U(0, H/2, t)/3$ is the average velocity of the flow passed the channel.

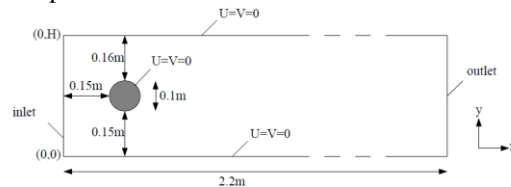


Figure 7. Geometry of 2D test cases with boundary conditions [12]

3.1. Inlet Boundary Bondition for Steady Flow

The inlet boundary condition is a flow boundary condition, with a fixed parabolic velocity profile.

$$U(0, y) = 4U_m y(H - y)/H^2, \quad V = 0 \quad (32)$$

To simulate this boundary condition, Zou and He boundary condition on a flow boundary is used.

$$f_{i_{\max}} = \frac{1}{3}(4f_{i_{\max-1}} - f_{i_{\max-2}}). \quad (33)$$

3.2. Outlet Boundary Condition

Since the gradients of flow variables at the outlet boundary are small temporally and spatially we can easily set these gradients to zero and extrapolate the distribution functions for the outlet boundary nodes [13].

By setting the first partial derivative of distribution function to zero and using second-order differencing the following relation is obtained for the distribution function:

3.3. Grid Dependency Study for Steady Flow

In order to study grid dependency, we solve the problem of the two-dimensional flow with $Re=20$ over a circular cylinder in a channel by using different grids. The results are shown in table 1. To obtain this table FH boundary condition is used for solid curved boundaries and Zou and He boundary condition is used for inlet and wall boundaries of the channel. By comparing the obtained results with each other the suitable resolution can be chosen.

Table 1. Drag and lift coefficients of a fixed circular cylinder in a flow channel ($Re=20$, $Ma=0.1$) with different resolutions

Resolution	Lattice Spacing ($\Delta x=\Delta y$) [m]	τ Relaxation Parameter	Boundary Treatment	Inlet & Channel Wall Boundary Treatment	C_D	C_L
221×42	0.01	0.5577	FH	Zou & He	Diverged	Diverged
441×83	0.005	0.6154	FH	Zou & He	5.616	0.011
661×124	0.00333	0.6732	FH	Zou & He	5.611	0.010
881×165	0.0025	0.7309	FH	Zou & He	5.609	0.010
1101×206	0.002	0.7886	FH	Zou & He	5.609	0.010

According to table 1 we choose the resolution 881×165 for flow domain. By using this resolution for flow domain the numerical results are not dependant on the number of grids anymore and according to figure 7 which shows the geometry of the flow the diameter and the center of the cylinder are 20lu and (81,81), respectively.

3.4. Numerical Results for a Two-dimensional Steady Flow

The following quantities have been computed for the steady flow: drag coefficient (C_D), length of recirculation zone (L_a). The results for drag coefficient and length of recirculation zone have been written in table 2.

Table 2. Percentage error for C_D and L_a for a steady flow ($Re=20$, $Ma=0.1$) compared with results reported in [12]

Boundary Treatment	C_D	Drag Error (%) with Lower Bound	Drag Error (%) with Upper Bound	L_a	L_a Error (%) with Lower Bound	L_a Error (%) with Upper Bound
FH	5.609	0.7	0.3	0.0817	2.9	4.1
Mass Conserving FH	5.684	2.0	1.6	0.0843	0.1	1.0
OSIF	6.211	11.5	11.1	0.0853	1.3	0.1

According to table 2 FH and Mass conserving FH boundary conditions show smaller error percentage than OSIF boundary condition which means, OSIF boundary condition is not able to meet conservation of momentum. So among these three

boundary conditions, FH and Mass conserving FH boundary conditions can show acceptable results for a steady flow.

4. Unsteady Two-dimensional Flow with Re=100 Over a Circular Cylinder in a Channel

For unsteady flows in which frequency plays a great roll, in addition to the previous non-dimensional numbers another non-dimensional number is used which is known as Strouhal number and is defined as [12]:

$$St = Df / \bar{U}, \quad (34)$$

where f is the frequency of vortex production.

4.1. Inlet Boundary Condition for Unsteady Flow

The inlet boundary condition is a flow boundary condition with a fixed parabolic velocity profile, the same as the steady flow:

$$U(0, y) = 4U_m y(H - y) / H^2, \quad V = 0 \quad (35)$$

In here, Zou and He boundary condition on a flow boundary is also used to simulate this boundary condition.

4.2. Outlet Boundary Condition for Unsteady Flow

The same boundary condition for steady flow is used for outlet boundary in unsteady flow.

4.3. Numerical Results for a Two-dimensional Unsteady Flow

The following quantities have been computed for the unsteady flow: drag coefficient (c_D) as a function of time, maximum drag coefficient $c_{D_{\max}}$, maximum lift coefficient $c_{L_{\max}}$ and Strouhal number (St). The results for unsteady flow (Re=100, $U_{\max}=0.1$) have been shown in table 3. Table 3, consists of maximum drag coefficient $c_{D_{\max}}$ and Strouhal number. FH boundary condition has been used for curved solid boundaries in table 3.

Table 3. Percentage error for $c_{D_{\max}}$ and $c_{L_{\max}}$ for unsteady flow (Re=100, $U_{\max}=0.1$) compared with results reported in [12]

Boundary Treatment	$c_{D_{\max}}$	Drag _{max} Error (%) with Lower Bound	Drag _{max} Error (%) with Upper Bound	St	St Error (%) with Lower Bound	St Error (%) with Upper Bound
FH	3.3130	2.8	2.2	0.303	2.7	0.6
Mass conserving FH	3.3053	2.6	2.0	0.303	2.7	0.6
OSIF	3.9590	22.9	22.1	0.301	2.0	1.3

As can be seen from table 3, OSIF boundary condition shows unacceptable error in comparison with the other two boundary conditions.

5. Unsteady Flow due to Translational Oscillation of a Circular Cylinder

In order to model moving curved solid boundary, the flow over a circular oscillating cylinder is simulated. Velocity profiles and exerted forces on the simulated cylinder are compared with benchmark results of H. Dutsch, F. Durst, S. Becker and H. Lienhart. For an oscillating motion a non-dimensional number is defined known as Keulegan-carpenter number [14]:

$$KC = \frac{U_{\max}}{fD}, \quad (36)$$

where U_{\max} is the maximum velocity of cylinder, D is the diameter of cylinder and f is the frequency of oscillation. The Reynolds number in this part is defined as:

$$Re = \frac{UD}{\nu}, \quad (37)$$

where, ν is the cinematic viscosity of the fluid. In the present study the translational motion $u_c(t)$ is given by the harmonic oscillation:

$$u_c(t) = -U_{\infty} \cos\left(\frac{2\pi}{T}t\right),$$

$$v_c(t) = 0. \quad (38)$$

where u_c and v_c are the velocity of center of cylinder, U_{∞} is the amplitude of the oscillation and T is the period of the oscillation. The fluid around the cylinder is at first stationary, as the cylinder starts to oscillate the fluid over the cylinder initiates to a semi-steady flow. The flow around an oscillating cylinder can be complex, showing vortex structures and mechanisms with different properties and different behaviors, but with parameter set of the present investigation, Re = 100 and KC = 5, a street of two symmetric and counter-rotating vortices of apparently the same

magnitude of strength were generated in front and back of the cylinder (figure 8).



Figure 8. Flow visualization for Re=100 and KC=5 [14]

The computational domain which is going to be simulated is shown in figure 9.

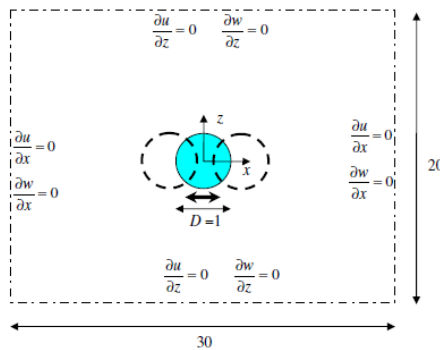


Figure 9. Sketch of the computational domain for a circular cylinder oscillating in-line in a quiescent fluid. The cylinder is initially set at the center of the domain [15]

5.1. Boundary Condition for Curved Solid Boundaries

For curved solid boundaries only FH and mass conserving FH boundary conditions are used because according to tables 2 and 3 they offer the smallest error percentage for curved solid boundaries.

5.2. Boundary Conditions for Computational Domain

For right, left, down and above boundary conditions of the computational domain, first-degree extrapolation using second-order differencing are used. By using extrapolation boundary condition an infinite flow domain is trying to be simulated.

$$\frac{\partial f}{\partial x} \Big|_{i_{\max}} = -\frac{3f_{i_{\max}} - 4f_{i_{\max}-1} + f_{i_{\max}-2}}{2\Delta x} = 0 \Rightarrow f_{i_{\max}} = \frac{1}{3}(4f_{i_{\max}-1} - f_{i_{\max}-2}). \tag{39}$$

5.3. Grid Dependency Study for Oscillating Cylinder

In order to study grid dependency of the problem of oscillating circular cylinder, the problem is going to be solved with different resolutions and by

comparing the results with the benchmark results the suitable resolution can be chosen for the flow domain. Table 4 compares the maximum drag coefficient of translational oscillating cylinder with different resolutions. The boundary condition which is used for table 4 is FH boundary condition.

Table 4. Maximum drag coefficient of translational oscillating cylinder with different resolutions

Resolution	Lattice Spacing ($\Delta x = \Delta y$) [m]	τ Relaxation Parameter	Boundary Treatment	$C_{D\max}$
601×401	0.0005	0.5346	FH	3.39
901×601	0.00033	0.5519	FH	3.35
1201×801	0.00025	0.5692	FH	3.33
1501×1001	0.0002	0.5866	FH	3.33

As can be seen from table 4 by choosing the resolution 1201×801 for flow domain the numerical results are not dependant on the number of grids anymore. By choosing this resolution for flow domain, the diameter and the center of the cylinder are 40lu and (601, 401), respectively, according to figure 9.

5.4. Numerical Results for Semi-steady Flow due to a Translational Oscillating Cylinder

The numerical results obtained for semi-steady flow due to the translational oscillating cylinder and also the numerical benchmark results of Duetsch et al. are shown in figures 10 to 12. At first the numerical results obtained using FH boundary condition for curved solid boundaries are shown. In figure 10, drag coefficient is drawn for the oscillating cylinder as a function of time and is compared with the benchmark numerical results of Dutsch et al.

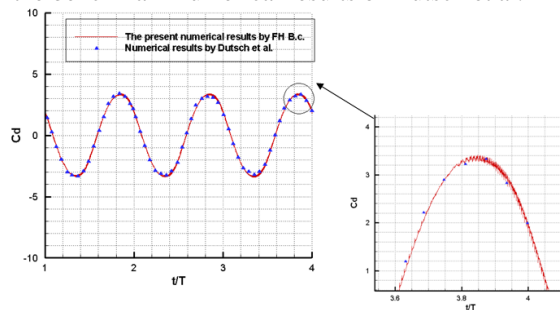


Figure 10. Drag coefficient as a function of time. ▲: numerical results of Dutsch et al. [14]; —: numerical results of the present study using FH boundary condition

Figure 11 shows the velocity profile of the flow domain in three different cross sections ($x = x_0 - 0.6D$, $x = x_0$, $x = x_0 + 0.6D$) and at temporal phase $t = nT + T/2$.

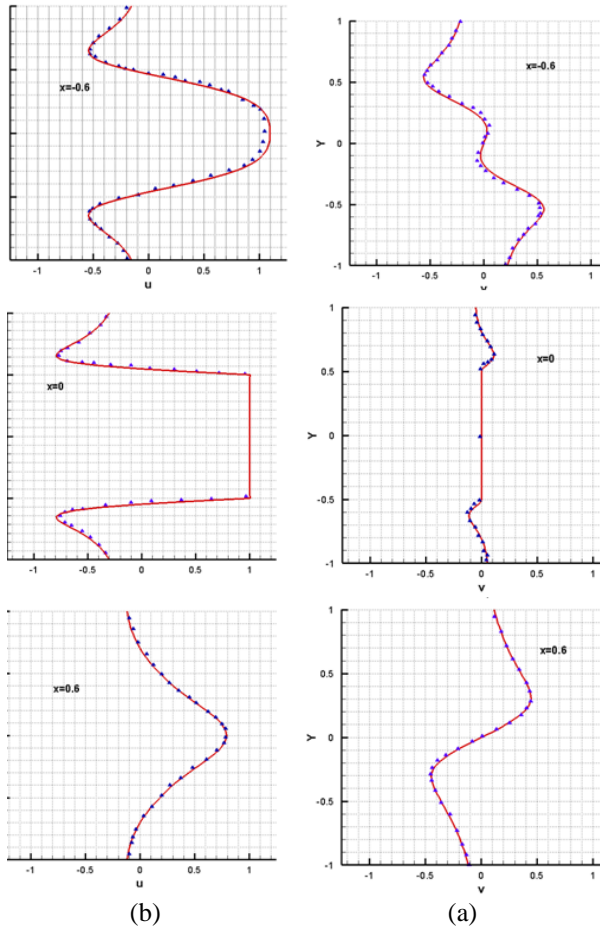


Figure 11. Comparison of velocity components in three different cross sections, in temporal phase $t = nT + T/2$. \blacktriangle : numerical results of Dutsch et al. [14]; $—$: numerical results of present study by using FH boundary condition for curved solid boundary (a) horizontal velocity component (b) vertical velocity component

Vorticity contours at different time cross sections ($t = T$, $t = T + 0.2T$, $t = T + 0.5T$ and $t = T + 0.8T$) of a period for $Re = 100$ and $KC = 5$ are shown in figure 12.

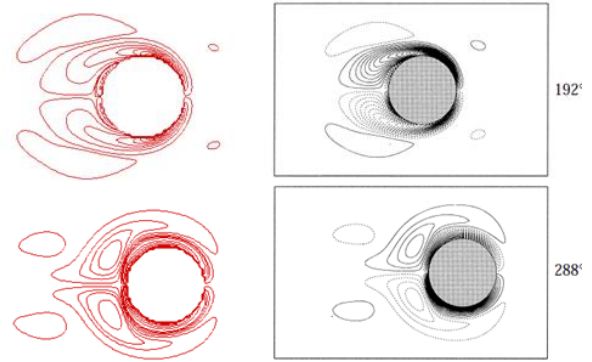
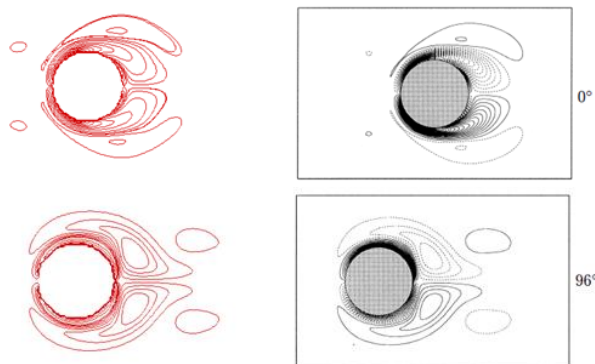


Figure 12. Velocity contours for $Re = 100$ and $KC = 5$. Right: numerical results of Dutsch et al. [14]. Left: numerical results of the present study

Numerical results obtained for flow domain of oscillating cylinder by using mass conserving FH boundary condition are shown in figures 13 and 14. In figure 13, drag coefficient is drawn as a function of time as is compared with numerical benchmark results of Dutsch et al.

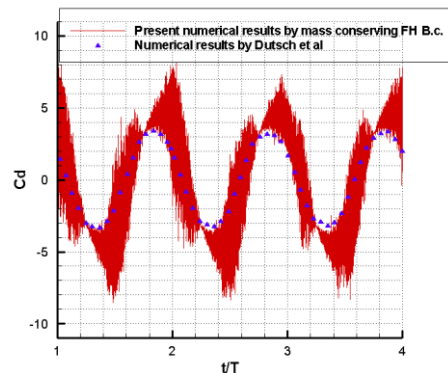


Figure 13. Drag coefficient as a function of time. \blacktriangle : numerical results of Dutsch et al. [14]; $—$: numerical results of the present study using Mass conserving FH boundary condition

Figure 14 shows the velocity profile of the flow domain in three different cross sections ($x = x_0 - 0.6D$, $x = x_0$, $x = x_0 + 0.6D$) and at temporal phase $t = nT + T/2$.

As can be seen in figures 13 and 14 numerical results obtained for velocity profile and drag coefficient as a function of time by using Mass conserving FH boundary condition are with unwanted fluctuations, which means that the mass conserving boundary condition cannot model moving curved solid boundaries accurately.

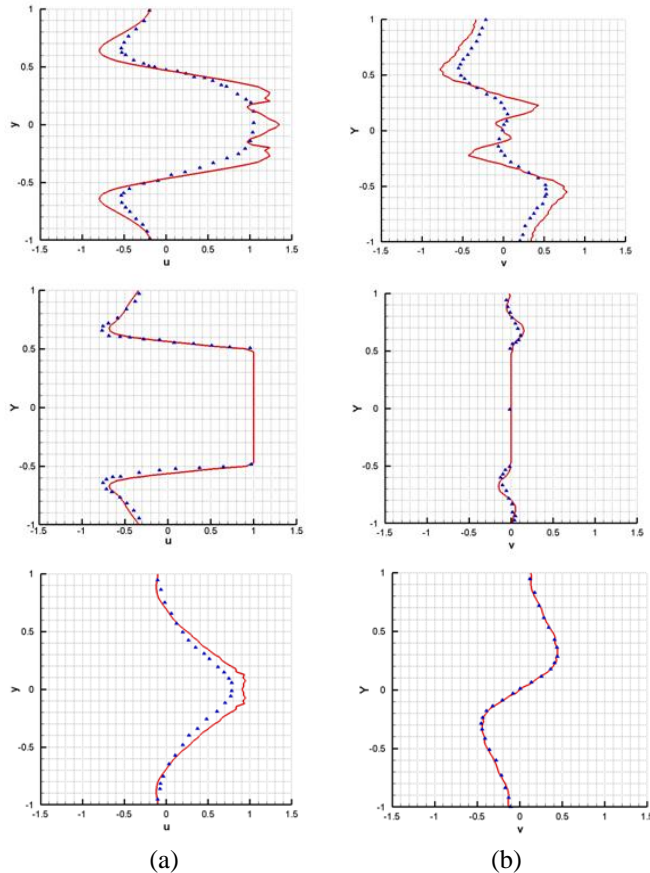


Figure 14. Comparison of velocity components in three different cross sections and in temporal phase $t = n.T + T/2$. \blacktriangle : numerical results of Dutsch et al. [14]; $—$: numerical results of present study by using Mass conserving FH boundary condition for curved solid boundary (a) horizontal velocity component (b) vertical velocity component

6. Conclusion

We can come to this conclusion that mass conserving FH boundary condition, in despite of convincing conservation of mass and momentum for stationary solid boundaries simultaneously, it cannot convince conservation of momentum for moving solid boundaries. The inability of mass conserving FH boundary condition in convincing conservation of momentum for moving solid boundaries is a topic which is not reported in literature, because mass conserving FH boundary condition used to be applied for stationary solid boundaries.

The probable reason why mass conserving FH boundary condition is not able to fulfill conservation of momentum for moving solid boundaries is the virtual compressibility of lattice Boltzmann method. In order to simulate a moving body the virtual compressibility of lattice Boltzmann method becomes more obvious, because during time

marching some solid nodes will change into fluid node and some fluid nodes will change into solid nodes. The density of a fluid node which has been changed from a solid node is assumed as the average density of the neighboring fluid nodes and its real density is not evaluated. So, at each time step, mass conserving FH boundary condition tries to maintain different total mass. Therefore, density fluctuation becomes more obvious for a problem which deals with moving bodies.

According to this study we can conclude that FH boundary condition offers more acceptable and more accurate results for moving curved solid boundaries compared with mass conserving FH boundary condition and OSIF boundary condition. So, in order to model moving curved solid boundary in simulation of applicational problems, we can easily trust on the results obtained from correct coding of FH boundary condition.

Corresponding Author:

Dr. Mojtaba Beigzadeh-abbassi
 Department of Mechanical Engineering
 Sirjan University of Technology, Sirjan, Iran
 E-mail: m.r.beigzadeh@gmail.com

References

1. Aidun, C.K. and Clausen, J.R. Lattice-Boltzmann Method for Complex Flows. *Annu. Rev. Fluid Mech.* 2010; 42(1):439-472.
2. Filippova, O. and Hanel, D. Grid Refinement for Lattice-BGK Models. *J. Com. Phys.* 1998; 147(1): 219–228.
3. Bao, J., Yuan, P. and Schaefer, L. A Mass Conserving Boundary Condition for the Lattice Boltzmann Equation Method. *J. Comp. Phys.* 2008; 227(18): 8472–8487.
4. Kao, P.H. and Yang, R. J. An Investigation into Curved and Moving Boundary Treatments in the Lattice Boltzmann Method. *J. Comp. Phys.* 2008; 227(11): 5671–5690.
5. Luo, L.S. The Lattice Gas and Lattice Boltzmann Methods: Past, Present and Future. ICASE Report, NASA Langley Research Center, USA, 2002.
6. Sukop, M.C. and Thorne, D.T. Lattice Boltzmann Modeling, An Introduction to Geoscientists and Engineers, Springer, 2006.
7. Chen, Sh. and Doolen, G. D. Lattice Boltzmann Method for Fluid Flows. *Annu. Rev. Fluid Mech.* 1998; 30(1): 329–64.
8. Zhou, J.G. Lattice Boltzmann Methods for Shallow Water Flows. Springer-Verlag, Berlin, Heidelberg, 2004.
9. Mei, R., Luo, L.S. and Shyy, W. An Accurate Curved Boundary Treatment in the Lattice

- Boltzmann Method. *J. Comp. Phys.* 1999; 155(2): 307–330.
10. Zou, Q. and He, X. On Pressure and Velocity Boundary Conditions for the Lattice Boltzmann BGK Model. *Phys. Fluids J.* 1996; 9(6): 1591-1599.
 11. Deladisma, M.D. Accuracy and Enhancement of the Lattice Boltzmann Method for Application to a Cell-Polymer Bioreactor System. Ph.D. Dissertation, Dept. of Mech. Eng. Georgia Institute of Technology, 2006.
 12. Schafer, M. and Turek, S. Benchmark Computations of Laminar Flow around a Cylinder. *Lehrstuhl fuer Stroemungsmechanik, Universitaet Erlangen-Nuernberg*, 1996.
 13. Chen, S., Martínez, D. and Mei, R. On Boundary Conditions in Lattice Boltzmann Methods. *Phys. Fluids J.* 1996; 8(9): 1788-1802.
 14. Dutsch, H., Durst, F., Becker, S. and Lienhart, H. Low-Reynolds-number Flow around an Oscillating Circular Cylinder at low Keulegan–carpenter Numbers. *J. Fluid Mech.* 1998; 360(1): 249-271.
 15. Shen, L., Chan, E.S. and Lin, P. Calculation of Hydrodynamic Forces Acting on a Submerged Moving Object Using Immersed Boundary Method. *J. Computers & Fluids* 2009; 38(3): 691–702.

2/21/2012